Lawrence Berkeley National Laboratory

Lawrence Berkeley National Laboratory

Title
Status of experimental data base development relevant to space radiation transport and protection

Permalink
https://escholarship.org/uc/item/45v3m7gn

Authors
Heilbronn, Lawrence H.
Guetersloh, Stephen
Zeitlin, Cary
et al.

Publication Date
2004-04-01

eScholarship.org

Powered by the California Digital Library
University of California

Status of experimental data base development relevant to space radiation transport and protection

L. Heilbronn, S. Guetersloh, J. Miller and C. Zeitlin

Lawrence Berkeley National Laboratory

DISCLAIMER

ABSTRACT

This report describes the highlights and progress made in a program of measurements studying radiation transport through materials of interest to NASA. All measurements were preformed at accelerator facilities, primarily using GCR-like heavy-ion beams incident upon various elemental and composite targets. Both primary and secondary particles exiting the target were measured. The secondary particles include both charged particles and neutrons. These measurements serve as useful benchmarks and input to transport model calculations.

INTRODUCTION

Humans engaged in long term missions in space face health risks from exposure to a radiation environment that consists of GCR, SEP, and in the case of low-Earth orbital missions, albedo neutrons and charged particles in trapped belts. Reduction of that risk while keeping mission costs reasonable relies on optimizing shielding design in the early planning stages of those missions. Shielding design incorporates calculational tools that include transport models, biological response models, and engineering models that allow the use of the calculations in computer-based, 3-D geometrical design codes. NASA is supporting research into the development of radiation transport codes that will be used in shielding design. Part of that effort is to acquire data at ground-based accelerator facilities that will support the development and validation of various transport model calculations. The ultimate goal of the ground-based research is to provide as complete of a description of the secondary radiation field created when components of the GCR and SEP pass through materials used in space-related activities (such as spacecraft shielding and habitat shielding on the surface of the moon and Mars). The focus of the measurements over the past ten years has been on the production of charged-particle secondaries (excluding pions) and neutrons. These experiments have provided modelers working on GCR transport model calculations with relevant data sets used to test and improve the models. The highlights of the research will be reported, along comparisons of the data with both one-dimensional semi-empirical models (such as NUCFRG2) and three-dimensional Monte-Carlo models (such as PHITS).

EXPERIMENTAL RESULTS

CHARGED PARTICLE EXPERIMENTS – Table I shows a complete listing of the beams and targets used for the charged-secondary particle measurements. The beam energies (in MeV/nucleon) represent the energy at extraction in the accelerator. Often, the beam energy on target is less due to energy loss in components along the beam line that lie between the extraction point and the target.

Listed with each target are the areal densities (in g/cm^2) used in each measurement. Most of the targets were composed of a single element; however, some complex targets (such as ISS wall materials and space suit materials) were also used. The "Marsbar" target is a 5.0 g/cm^2-thick brick made of 85% simulated Martian regolith and 15% polyethylene. The vast majority of the targets were thin enough to facilitate production cross-section measurements. Multiple thicknesses of each target were run to estimate and minimize systematic uncertainties in the cross sections due to multiple scattering and secondary interactions in the target.

All measurements were made with a Si-detector telescope arranged in various configurations. Examples of the detector configurations may be found in Refs. 1-5. The majority of the measurements were done at 0 degrees (relative to the incoming direction of the beam). Some off-axis measurements were also made out to 10°

Table I – Beams (energies in MeV/nucleon) and targets (thicknesses in g/cm^2) used in the charged-secondary particle measurements.

Beam (Energy)	Targets (areal densities in g/cm^2)
H (40)	Space suit materials
H (55)	ISS wall components, space suit materials
H (155)	CH_2 (11.8, 13.5), Phantom (head and torso)
H (250)	CH (1.05, 2.4, 5.0, 10.5, 21.0, 29.0, 30.5, 31.8, 32.1, 32.45, 32.6), Al (6.86), Tissue equivalent plastic (5.4)
He (230)	C (5.50), CH_2 (4.81), Al (5.64), Cu (5.68), Sn (5.90), Pb (7.98)
C (290)	C (1.995, 3.99), CH_2 (1.98, 2.824), Al (1.74, 1.755, 3.24, 3.51), Cu (2.81, 4.47, 5.63, 7.17), Sn (2.24, 5.97),Ta (10.04), Pb (3.6, 6.8, 10.2), Marsbar, ISS wall
C (400)	C (1.995, 3.6, 3.99), CH_2 (1.98, 2.824), Al (1.62, 3.24, 3.5), Cu (4.45, 5.58, 7.17), Sn (3.655, 5.97), Ta (10.04), Pb (4.54, 6.78, 7.21, 10.2), Marsbar
N (290)	C (3.8), CH_2 (1.98, 2.824), Al (4.05), Cu (4.475), Sn (3.672), Pb (4.536)
N (400)	C (1.99, 3.99), CH_2 (1.98, 2.824), Al (1.62, 3.24), Cu (4.48, 7.16), Sn (3.67, 5.90), Ta (9.95), Pb (2.27, 6.80, 10.2)
O (290)	C (1.26, 1.99), CH_2 (0.957, 1.98), Al (2.7), Cu (4.475), Sn (3.67), Pb (3.4)
O (400)	C (1.995), CH_2 (1.98), Al (1.62, 3.24), Cu (4.48), Sn (5.89), Pb (10.22)
Ne (290)	C (2.7), CH_2 (1.98), Al (2.7), Cu (2.842), Sn (3.67), Pb (3.42)
Ne (400)	C (1.08, 1.99), CH_2 (0.1, 1.98, 2.824), Al (2.42, 3.24), Cu (2.69, 4.48), Sn (2.2, 3.67), Pb (3.40, 4.52), H_2O
Ne (600)	Li (1.86, 2.80), C (1.99, 3.99), CH_2 (1.98, 2.824, 3.09), Al (3.24), Cu (4.48, 7.17), Sn (3.67, 5.97), Ta (10.04), Pb (6.78, 10.2), Marsbar
Si (290)	C (1.99), CH_2 (1.08, 1.98), Al (1.89), Cu

Target	
	(1.79), Sn (2.22), Pb (2.27)
Si (400)	C (1.08, 1.99, 2.66), CH_2 (1.98, 2.824), Al (2.42, 3.24), Cu (2.79, 5.527), Sn (2.22, 3.73), Pb (2.26, 3.39, 3.402)
Si (600)	C (1.31, 1.5, 1.995, 3.99), CH_2 (0.96, 1.98, 2.824), Al (1.62, 2.43, 3.24), Cu (2.79, 3.58, 4.45, 7.17), Sn (1.46, 3.73, 5.97), Ta (10.04), Pb (4.56, 6.78, 7.14, 10.2), spacesuit material
Si (800)	C (2.25, 3.6), CH_2 (2.824), Al (3.78), Cu (5.27, 4.475), Sn (3.65), Pb (4.52, 6.78)
Si (1200)	C (1.62, 1.95, 3.99), CH_2 (1.98, 2.824), Al (3.24), Cu (4.45, 7.14), Sn (3.73, 5.97), Pb (6.8, 10.2)
Ar (400)	C (1.3, 1.99), CH_2 (1.98, 2.824), Al (1.08, 1.62), Cu (2.7, 5.53), Sn (2.22, 5.89), Pb (2.2, 6.78, 10.22)
Ar (650)	C (1.99, 3.6), CH_2 (1.98, 2.824), Al (2.7, 4.05), Cu (3.73, 4.475), Sn (3.65, 5.8), Pb (5.67)
Fe (400)	C (2.93), CH_2 (1.98, 3.816, 7.87), Al (1.62), Cu (1.79, 3.74), Sn (2.22), Pb (2.268)
Fe (500)	Li (1.86), C (1.49, 1.98), CH_2 (1.27, 1.98), Al (1.89, 2.43), Cu (1.79, 2.67), Sn (1.45, 2.22), Pb (2.23, 2.27)
Fe (600)	C (1.95, 1.995, 3.99), CH_2 (1.98, 2.824, 5.0, 6.3), Al (1.62, 1.76, 2.7, 3.51), Cu (2.7, 2.81, 4.48, 5.63), Sn (3.655), Pb (3.6, 7.21, 10.76), LiHP (5.0), LiF (5.0),
Fe (800)	C (3.5, 5.4), CH_2 (2.824, 4.81), Al (2.7, 4.98), Cu (2.84, 4.48), Sn (5.1), Pb (6.85)
Fe (1000)	CH_2 (4.8)
Fe (1087)	C (0.5, 1.68, 1.95, 3.33, 3.90), CH_2 (1.98, 2.824, 3.6, 4.6, 5.0, 6.3, 9.35, 9.99, 13.1, 13.5, 17), Al (0.43, 1.755, 3.51, 7.02, 11.6), Cu (0.35, 2.81, 4.48, 5.63, 5.86, 7.17 11.3, 19.5), Sn (3.655, 5.90), Ta (10.04), Pb (3.6, 6.74, 7.21, 10.21, 10.76, 14.41), Boron epoxy (5.0), Graphite epoxy (5.0), PE/LI (5.0), PETI-5 (5.0), PE+B (5.0), Marsbar, ISS wall, lucite (1.28, 22.0)
Ti (1000)	C (1.905, 3.5, 3.81, 5.4, 20), CH_2 (2.824, 4.8), Al (2.7, 4.05), Cu (3.73, 5.68), Sn (3.67, 5.13), Pb (3.402, 4.56, 5.67), lucite (23.0)

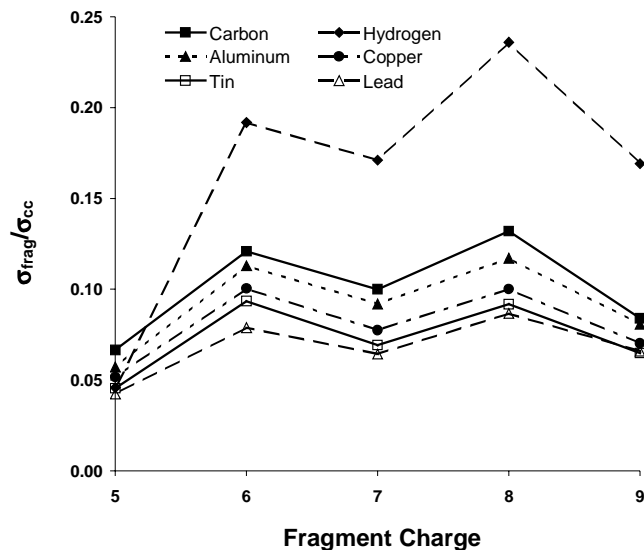nuclear structure effects manifested in final-state interactions.

Figure 1. The ratio of fragment-production cross sections to total charge-changing cross sections for the indicated targets. The ratios are shown for fragment charges 5-9.

Table II shows the total charge-changing cross sections for 600 MeV/nucleon Ne interactions in the indicated targets. The second column shows the measured cross sections, and the third column shows NUCFRG2 calculations[7] of the same cross sections. Agreement between data and calculation is quite good. Comparisons with other data sets also show good agreement with NUCFRG2 calculations[2,5,6].

Table II – Measured charge changing cross sections (second column, in mb) and calculated cross sections (third column) for 600 MeV/nucleon Ne interactions in the indicated targets.

Target	σ_{cc} (mb)	NUCFRG2
H	299 ± 9	331
C	987 ± 29	1000
Al	1354 ± 41	1374
Cu	1981 ± 59	1979
Sn	2537 ± 76	2624
Ta	3179 ± 95	3210
Pb	3396 ± 102	3429

In general, NUCFRG2 also reproduces the secondary-fragment production-cross-sections well. However, QMSFRG[8] does a better job in reproducing the enhancement of even-Z fragments that is seen in the data, at least in the data sets analyzed thus far.

Analysis of the data sets with composite targets, such as ISS wall materials and spacesuit materials, has focused on extracting dosimetric quantitites to test the effectiveness of those materials in regards to radiation

Results from selected 1087 MeV/nucleon Fe, 600 MeV/nucleon Fe, and 600 MeV/nucleon Ne measurements have been published[1-5]. Preliminary results from selected 400 MeV/nucleon C, N, and Si and 600 and 1000 MeV/nucleon Si measurements are available in a LBNL report[6]. Figure 1 shows the ratio of the fragment production cross section to the total charge-changing cross section for 600 MeV/nucleon Ne interactions in the indicated targets. The hydrogen target data was generated by subtracting the carbon-target data from the polyethylene-target data. As the mass of the target decreases, the cross-section ratios increase. Also evident in Fig. 1 is the "odd-even" effect, where elements with even atomic number are produced in greater numbers than their odd-atomic-numbered neighbors. This effect has been noted in other data sets as well[1-3,5,6], and is believed to be a consequence of

protection. Thus far, analysis has been completed on data sets with beams energies above 600 MeV/nucleon[5], and it has been found that nuclear fragmentation leads to a net decrease in dose and dose equivalent per incident ion. Consistent with model predictions, hydrogen-rich materials appear to provide the largest reductions in dose for a given shield mass. Calculations also predict that for lower incident energies (below 400 MeV/nucleon), the increased ionization energy loss of primary ions that do not undergo a nuclear interaction leads to an increase in some dosimetric quantities. Analysis of the data sets with beam energies below 400 MeV/nucleon will test that prediction.

SECONDARY NEUTRON EXPERIMENTS – Table III shows the beam/target systems used to study the production of secondary neutrons from heavy-ion interactions. Both thin-target (cross sections) and stopping-target (thick target yields) measurements have been carried out. Target thicknesses in Table III for the thin target measurements are in units of g/cm^2. Target thicknesses labeled "stop" are thick enough to stop the incident beam. Beam energies are in units of MeV/nucleon. All thin-target experiments measured neutrons produced between 5 and 80 degrees. The stopping target measurements varied from experiment to experiment, but in general measured neutrons between 5 and 160 degrees.

Beam (energy)	Target (thickness)
He (155)	Al (stop)
He (230)	Al (5.4), Cu (5.37)
C (155)	Al (stop)
C (290)	C (1.8), Cu (4.475), Pb (2.268), Marsbar (5.0)
C (400)	Li (3.048), C (3.568, 9.0), Al (3.985), Cu (4.475, 13.4), Pb (4.536, 9.0)
N (400)	C (1.784), Cu (2.688)
Ne (400)	C (1.8), Cu (4.475), Pb (2.268), ISS wall (2.97)
Ne (600)	Li (2.80, 2.968), C (3.6), CH$_2$ (2.4, 2.74), Al (3.24, 3.985), Cu (4.475), Pb (4.536), Marsbar (5.0)
Si (600)	C (1.80), Cu (3.58), Pb (4.536)
Ar (400)	C (0.72), Cu (1.34), Pb (1.70)
Ar (560)	C (1.08), Cu (1.79), Pb (2.268), Marsbar (5.0)
Fe (500)	Li (0.903), CH$_2$ (0.957, stop), Al (1.285)
Kr (400)	Li (0.469), C (0.549), CH$_2$ (0.46), Al (0.54), Cu (0.895), Pb (1.021)
Xe (400)	Li (0.477), C (0.280), CH$_2$ (0.201, 0.355), Al (0.256), Cu (0.448), Pb (0.567)
Nb (272)	Al (stop), Nb (stop)
Nb (435)	Nb (stop)

Most of the charged-particle secondary fragment spectrum is directed along the beam axis in high-energy heavy-ion interactions. This is particularly true for the heavier-mass fragments (roughly greater than about ½ the mass of the incoming ion). One-dimensional models

adequately describe such spectra and can be used to describe those aspects of GCR transport through shielding materials. However, nucleon and light-fragment secondary spectra are spread out over all space (in the laboratory reference frame), and as such require 3-dimensional models to describe their production. The secondary-neutron production cross-section and thick-target data measured here provide a stringent test of such models.

Figure 3 shows neutron production spectra from 290 MeV/nucleon C interacting in the 5 g/cm^2 Marsbar target. Spectra are offset by the indicated factors of 10 in order to clearly separate the data at each angle. The spectra at forward angles are dominated by a peak centered near the beam velocity. Projectile fragmentation is the dominant mechanism for the production of those neutrons. As the angle increases, the contribution from projectile fragmentation decreases and the contributions from the decay of the overlap region and target remnant become the dominant sources of neutrons. These results are consistent with other neutron spectra measured from heavy-ion interactions[8]. The histograms show PHITS calculations[9] of the spectra. In general, the calculations reproduce the data well. Most codes modified to include heavy-ion interactions have had problems reproducing the peak from projectile fragmentation at forward angles. The PHITS calculations shown in Fig. 3 show good agreement with the forward angle data, which indicates the improvement modelers have made in the last ten years of heavy-ion transport model calculations.
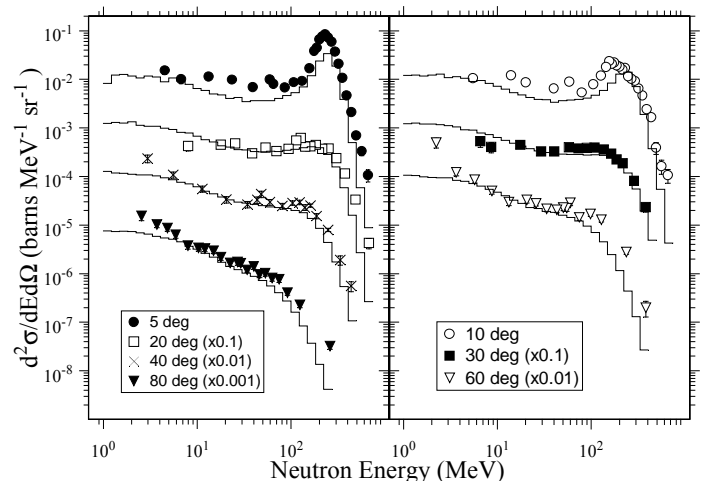

Figure 3 – Neutron spectra from 290 MeV/nucleon C + Marsbar interactions. Spectra are offset by the indicated factors of 10. The histograms show the results from PHITS calculations.

CONCLUSION

A catalog of heavy-ion induced secondary-particle measurements made at accelerator facilities has been

presented. These data are important in the development and verification of GCR transport model calculations used to develop viable shielding options for long-term operations in space. Although much of the data is still being analyzed, some trends are already evident from the analyses that have been completed. The "odd-even" effect in secondary charged particle production show the effects of nuclear structure in final state interactions. For primary GCR energies above 400 MeV/nucleon, the data verify that nuclear interactions in the shielding materials reduce the dose and dose-equivalent behind shielding. Neutron data illustrate the 3-dimensional aspects of nucleon and light-ion spectra. Comparisons of these data with current models show the improvements made in model calculations of high-energy heavy-ion model calculations.

ACKNOWLEDGMENTS

REFERENCES

1. C. Zeitlin, J. Miller, L. Heilbronn, K. Frankel, W. Gong, and W. Schimmerling, Radiat. Res. **145**, no. 6, 655-665, (1996).
2. C. Zeitlin, L. Heilbronn, J. Miller, S. E. Rademacher, T. B. Borak, T.R. Carter, K. A. Frankel, C. E. Stronach., Phys. Rev. C **56**, 388-397 (1997).
3. J. Miller, C. Zeitlin, L. Heilbronn, T. B. Borak, T. Carter, K. Frankel, A. Fukumura, T. Murakami, S. Rademacher, W. Schimmerling, and C. Stronach, Acta Astr. **42**, 384-389 (1998).
4. C. Zeitlin, A. Fukumura, L. Heilbronn, Y. Iwata, J. Miller, and T. Murakami, Phys. Rev. C **64** 024902.
5. J. Miller, C. Zeitlin, F. A. Cucinotta, L. Heilbronn, D. Stephens and J. W. Wilson, Radiat. Res. **159**, 381-390 (2003).
6. C. Zeitlin, L. Heilbronn, J. Miller, A. Fukumura, Y. Iwata, T. Murakami, J. MacGibbon, L. Pinsky and T. Wilson, LBNL report 48879 (2001).
7. J. W. Wilson, J. L. Shinn, L. W. Townsend, R. K. Tripathi, F. F. Badavi, and S. Y. Chun, Nucl. Instr. Meth. B **94**, 95 (1994).
8. Y. Iwata, T. Murakami, H. Sato, H. Iwase, T. Nakamura, T. Kurosawa, L. Heilbronn, R.M. Ronningen, K. Ieki, Y. Tozawa, and K. Niita, Phys. Rev. C **64**, 054609 (2001).
9. H. Iwase, K. Niita and T. Nakamura, Journ. Nucl. Sci. Tech., **39**, 1142-1151 (2002).

CONTACT

Lawrence Heilbronn
MS 74-197
Lawrence Berkeley National Laboratory
Berkeley, CA 94720
USA
LHHeilbronn@lbl.gov

DEFINITIONS, ACRONYMS, ABBREVIATIONS

NASA – National Aeronautics and Space Administration
GCR – Galactic Cosmic Radiation (or Rays)
SEP – Solar Energetic Particle(s)
ISS – International Space Station
LBNL – Lawrence Berkeley National Laboratory